Annals of the University of Craiova, Mathematics and Computer Science Series
Volume 51(1), 2024, Pages 150–166, DOI: 10.52846/ami.v51i1.1753
ISSN: 1223-6934

Iterative Algorithm using Decoupling Method for third-order Tensor Deblurring

Karima El Qate, Souad Mohaoui, Abdelilah Hakim, and Said Raghay

Abstract. The present paper is concerned with exploiting an iterative decoupling algorithm to address the problem of third-order tensor deblurring. The regularized deblurring problem, which is mathematically given by the sum of a fidelity term and a regularization term, is decoupled into an observation fidelity and a denoiser model steps. One basic advantage of the iterative decoupling algorithm is that the deblurring problem is supervised by the efficiency of the denoiser model. Thus, we consider a patch-based weighted low-rank tensor with sparsity prior. Numerical tests to image deblurring are given to demonstrate the efficiency of the proposed decoupling based algorithm.

2020 *Mathematics Subject Classification.* Primary 60J05; Secondary 60J20.
Key words and phrases. Tensor deblurring, decoupling method, iterative algorithm, denoising, low-rank approximation, weighted sparsity.

1. Introduction

Image deblurring is one of the earliest and most classical inverse problems, in which the aim is to estimate the original clean image from the corresponding blurry and noisy image. Actually, intrinsic or extrinsic factors may lead to degradation in the quality of the acquired image, of which blur is one example. Blur is generally due to one of five types relative motion blur, camera shake blur, defocus blur, atmospheric turbulence blur, and intrinsic physical blur. It causes an image pixel to record light photons from multiple scene points. The deblurring problem usually models the object to be recovered as a vector of unknowns and the blurring operator as a matrix. Over the years, several novel approaches have been presented to deal with the 2D image deblurring problem driven by a variety of motivations [26, 3, 22, 23, 30, 7].

Recently, the development of modern imaging technologies has led to significant growth in the size of data. Thus, modeling multidimensionality is of great interest. In this vein, the use of tensors, the higher-order extension of matrices, has demonstrated a significant impact in modeling and handling high dimensional images and videos processing. Actually, multidimensional data has received considerable attention in a variety of areas such as signal and image processing, machine learning, and computer vision. Tensors are an important big data format, which play a notable role in a wide range of real-world applications including video inpainting [17] hyperspectral data recovery [19, 9], tensor completion [20, 11], fluorescence spectroscopy data analysis [10] and seismic data reconstruction [18]. For example, the problem of hyperspectral image deblurring aims at recovering sharp images with a large number of spectral

Received April 4, 2023. Accepted October 7, 2023.

channels from blurred and noisy observations. This problem can be seen as a third-order tensor restoration problem.

Mathematically, given an observed third-order tensor $\mathcal{Y} \in \mathbb{R}^{n_1 \times n_2 \times n_3}$, the problem of tensor deblurring can be expressed by the following equation:

$$\text{find } \mathcal{X} \ : \ \mathcal{Y} = \mathcal{K}(\mathcal{X}) + \mathcal{N} \tag{1}$$

where $\mathcal{K}$ is a bounded linear operator representing the blur, $\mathcal{X}$ is the original tensor, and $\mathcal{N}$ represents an additive white Gaussian noise. Recovering $\mathcal{X}$ from $\mathcal{Y}$ is called a linear inverse problem which, for most scenarios of practical interest, is ill-posed .i.e small changes in $\mathcal{Y}$ may lead to a huge deviation of the solution $\mathcal{X}$. The ill-posedness which is the most severe problem in image deblurring, is caused by either the direct operator does not have an inverse or it is nearly singular with noise sensitivity, or due to the ill-conditioned nature of the blur operator $\mathcal{K}$ [21]. To deal with ill-posedness, researchers have been developing new approaches, as well as enhancing the efficiency of optimization methods and algorithms. One of the most used models is the variational method which renders the solution unique and stable through the incorporation of regularization techniques. In order to regularize the solution $\mathcal{X}$, it is important to incorporate prior information on images. Formally, variational models for image processing in general consist of the sum of a data term and a regularization term:

$$\arg\min_{\mathcal{X}} \left\{ E(\mathcal{X}) \ = \ \frac{1}{2}\|\mathcal{Y} - \mathcal{K}(\mathcal{X})\|_F^2 \ + \ \lambda J(\mathcal{X}) \right\} \tag{2}$$

The first term refers to the fidelity term which measures the disparity between $\mathcal{K}(\mathcal{X})$ and the observation $\mathcal{Y}$, while the second is the regularization term that promotes certain solutions. The regularization parameter $\lambda \geq 0$ balances the contributions of the two terms.

1.1. Related works. Regarding the regularization methods, finding and modeling appropriate prior knowledge is one of the most important concerns. Thus, different choices lead to different reconstruction approaches. Particularly, for the deblurring problem diverse models have been developed during the last decades. Patch-based sparsity model assumes the sparsity of image under learned dictionaries [23, 29], which provides an effective characterization of natural images. The low-rank prior is another sparsity regularization in the domain of singular value decomposition (SVD). The low-rank approximation is an effective tool for high dimensional data modeling which has attracted more and more attention in several advanced imaging fields [**?**, 15, 2]. Nonlocal self-similarity prior characterizes the repetitiveness and the redundancy of textures and structures in images. The nonlocal methods have achieved better empirical results compared to some local regularization methods [14, 5]. Motivated by this, patch-based low-rank prior has recently gained a growing interest [13, 14, 29, 4]. The key point is that a group of similar patches can be well approximated by a low-rank matrix. This approach has already achieved fast and impressive results in bidimensional image recovery. For high dimensional data modeling, the low-rank modeling and the redundant non-local self similarities have attracted more and more attention in several applications [7, 14, 4, 31]. These models have been adopted successfully in several high-dimensional image recovery due to their simplicity. Indeed, multidimensional images have many repetitive local patterns, and a local patch can have many similar patches to it across the whole image. The low-rankness of a tensor is essential

to describe the intrinsic geometrical structure of these data. Patch-based low-rank models have shown their ability to exploit the spatial redundancy of computer vision data. In high dimensional data, considering both the spatial and spectral information and the correlation between them has attracted more and more attention in several reconstruction problems. To enhance the low-rankness structure in images, the nonlocal self-similarity via grouping similar patches has been considered in unified models leading to robust high-dimensional reconstruction approaches including, denoising, completion, deblurring, and super-resolution [4, 31]. In [4], authors introduced a low-rank restoration model for hyperspectral images based on a weighted operation for modeling the spatial nonlocal self-similarity and spectral correlation exhibited in adjacent bands. Further, they take the intrinsic sparsity of the core tensor into account by using a reweighting strategy which demonstrates to better encode the structure correlation. This model has been considered with subspace representation to remove the mixed noise in the hyperspectral image in [31]. On the other hand, with the great success achieved by deep learning models in several applications, image deblurring also benefits from this advancement. Therefore, several deep deblurring models with different deep architectures have been developed in recent years especially for blind deblurring problems [24, 30]. However, to the best of our knowledge, only one deep learning model has addressed the tensor deblurring problem [13] in which a deep convolutional network (ConvNet) structure has been employed as an image prior. This model proposed an image/tensor modeling method using a denoising-auto-encoder in combination with a multi-way delay-embedding transform.

Indeed, a good optimization algorithm has a critical role in producing accurate solutions. Thus, concerning the optimization methods used to solve (2), various computational algorithms based on convex analysis have been sprung up in recent years. The splitting theory has been among the successful techniques that have been exploited for building efficient deblurring algorithms. The alternating direction method of multipliers (ADMM) method has emerged as an efficient splitting tool to address several imaging inverse problems of the form (2). ADMM is an algorithm that attempts to solve a convex optimization problem by decoupling it into simple subproblems easier to solve.

In spite of the good results of splitting algorithms, the research for efficient image deblurring methods is still a great challenge. Recently, a new iterative method based on a decoupling technique has been introduced for 2D image deblurring problem [26]. This method has been shown to be particularly efficient for image restoration based on the model (2). Instead of the variable-based splitting technique, the iterative decoupling method presents another view of the splitting concept. It consists of decoupling the objective function; given by the sum of a fidelity term and a regularization term; into two iterative problems yielding simpler optimization problems. The two steps have been named differently, they have first been called denoising and the deblurring steps in [26] and the observation fidelity and the model fidelity steps for recovery problems [8]. Since the reconstruction task is supervised by the denoising step, we call the decoupling steps the observation fidelity and the denoiser model steps.

1.2. Contribution. Motivated by the success of the iterative decoupling method for image deblurring in the context of matrices, we are interested in extending this method for the third-order tensor deblurring problems. The deblurring process is controlled

by the denoiser model. The iterative decoupling presents a soft framework to easily integrate sophisticated denoisers. Therefore, in this paper, we consider the iterative decoupling method with the low-rank tensor regularization term [4]. In particular, we envisage the weighted low-rank tensor recovery model as a model denoiser. In contrast, by observing the decoupling property of the ADMM method used in [4], it is basically based on the splitting of variables using an auxiliary procedure. The ADMM method needs an auxiliary procedure to alternate between the minimization of the augmented Lagrangian function to exchanging intermediate results with adjacent subregions and updating the associated Lagrangian multipliers.

The remaining parts of this paper are organized as follows. In Section 2, some notions and definitions are introduced. In Section 3, we present the proposed iterative algorithm-based decoupled method for third-order tensor deblurring. Moreover, we introduce in detail the suggested denoising step, which is based on low-rank tensor learning. In Section 4, extensive numerical experiments are presented to validate the effectiveness of the proposed deblurring model. Finally, some concluding remarks are given in Section 5.

2. Notions and preliminaries

Throughout this work, we use calligraphy letters to denote tensors, e.g. $\mathcal{X}$, boldface uppercase letters to denote matrices, e.g., $\boldsymbol{X} \in \mathbb{R}^{m\times n}$, boldface lowercase letters to denote vectors, e.g., $\boldsymbol{x}_i \in \mathbb{R}^n$, and lowercase letters to denote scalars, e.g., x_{ij}. We denote a d-th-order tensor and its entries by $\mathcal{X} \in \mathbb{R}^{n_1\times\cdots\times n_d}$ and $x_{i_1\ldots i_d}$, respectively. Let $\boldsymbol{X}_{(k)} \in \mathbb{R}^{n_k\times(\Pi_{l\neq k}n_l)}$ denote the k-*th*-mode unfolding of tensor $\mathcal{X}$ for $k = 1,\ldots,d$, this transformation is called matrix unfolding.
The inverse operator of unfold is denoted as fold and defined as follows:

$$\mathcal{X} = \text{fold}_k\left(\boldsymbol{X}_{(k)}\right)$$

The Frobenius norm of a N-way tensor $\mathcal{X} \in \mathbb{R}^{I_1\times I_2\times\cdots\times I_N}$ is defined as

$$\|\mathcal{X}\|_F = \left(\sum_{i_1=1}^{I_1}\sum_{i_2=1}^{I_2}\cdots\sum_{i_N=1}^{I_N}|x_{i_1i_2\ldots i_N}|^2\right)^{\frac{1}{2}},$$

where $x_{i_1i_2\ldots i_N}$ is the $(i_1, i_2, \ldots, i_N)$-th element of the tensor $\mathcal{X}$.
The inner product of two same-sized tensors $\mathcal{X}$ and $\mathcal{Y}$ is defined as:

$$\langle\mathcal{X},\mathcal{Y}\rangle = \sum_{i_1,i_2,\ldots,i_N} x_{i_1i_2\ldots i_N}\cdot y_{i_1i_2\ldots i_n}$$

Definition 2.1 (mode-n tensor matrix product)**.** ([6])
The mode-n product $\mathcal{X} = \mathcal{Y}\times_n \boldsymbol{A}$ of a tensor $\mathcal{Y} \in \mathbb{R}^{J_1\times J_2\times\cdots\times J_N}$ and a matrix $\boldsymbol{A} \in \mathbb{R}^{I_n\times J_n}$ is a tensor $\mathcal{X} \in \mathbb{R}^{J_1\times\cdots\times J_{n-1}\times I_n\times J_{n+1}\times\cdots\times J_N}$, with elements

$$y_{j_1,j_2,\ldots,j_{n-1},i_n,j_{n+1},\ldots,j_N} = \sum_{j_n=1}^{J_n} g_{j_1,j_2,\ldots,j_N}a_{i_n,j_n}$$

Definition 2.2 (HOSVD)**.** ([6])
The HOSVD can be considered as a special form of Tucker decomposition which

decomposes an N-th order tensor $\mathcal{X} \in \mathbb{R}^{I_1 \times I_2 \times \cdots \times I_N}$ as

$$\mathcal{X} = \mathcal{D} \times_1 \boldsymbol{V}_1 \times_2 \boldsymbol{V}_2 \cdots \times_N \boldsymbol{V}_N$$

where $\boldsymbol{V}_n$, $(n = 1, 2, \cdots, N)$ are orthogonal matrices and the core tensor $\mathcal{D}$ is an all-orthogonal and ordered tensor of the same dimension as the data tensor $\mathcal{X}$.

Remark 2.1. For a tensor $\mathcal{X} \in \mathbb{R}^{I_1 \times I_2 \times \cdots \times I_N}$ and a matrix $\boldsymbol{V} \in \mathbb{R}^{I_n \times J_n}$, we have

$$\|\mathcal{X} \times_j \boldsymbol{V}\|_F^2 = \|\mathcal{X}\|_F^2, \ \forall \ \boldsymbol{V}^T\boldsymbol{V} = I$$

where $\times_j$ is mode-j tensor matrix product.

Theorem 2.1. *$\forall A \in \mathbb{R}^{m \times n}$, the following problem:*

$$\max_{U^T U = I} \langle A, U \rangle$$

has the closed-form solution $\hat{U} = BC^T$, where $A = BDC^T$ is the SVD decomposition of A.

Proof. The proof of Theorem 2.1 can be found in supplementary material of article [28]. □

3. Methods

We address in this section the tensor deblurring problem. By using the iterative decoupling method, we therefore, handle two simple steps, the observation-fidelity given by a smooth minimization problem addressing the deblurring task and a denoiser-model based on the chosen prior. As a regularization term, we consider the low-rank prior with sparse-nonlocal self similarity constraint used in DB-WLRTR method [4] to observe the merit of the iterative decoupling algorithm over the ADMM method by enhancing the DB-WLRTR deblurring model. Before introducing the proposed algorithm, we first briefly present an overview about the iterative decoupling method and the low-rank based nonlocal sparsity regularization term.

3.1. Iterative algorithm based decoupled method for third-order tensor deblurring. Generally, the deblurring problem is mathematically given by a minimization problem of the form (2) which is the sum of a smooth and a convex function. The decoupled method is an efficient algorithm for solving the problem (2) which has been recently introduced for image restoration. The main idea of this algorithm is to decouple the smooth and the convex functions into two simple minimization problems. By starting from an initial guess $\mathcal{X}^{(0)}$, the iterative method computes alternatively a sequence of iterates such that:

$$\begin{cases} \mathcal{P}_{\mathcal{K}} \ : & \hat{\mathcal{X}}^{(i)} = \arg\min_{\mathcal{X}} \|\mathcal{Y} - \mathcal{X} * \mathcal{K}\|_F^2 + \mu \|\mathcal{X} - \mathcal{X}^{(i-1)}\|_F^2 \\ \mathcal{P}_{\mathcal{J}} \ : & \mathcal{X}^{(i)} = \arg\min_{\mathcal{X}} \|\mathcal{X} - \hat{\mathcal{X}}^{(i)}\|_F^2 + \lambda \mathcal{J}(\mathcal{X}) \end{cases} \tag{3}$$

where $*$ designs the convolution operator, $\mathcal{K}$ is constructed from a linear shift-invariant point spread function (PSF) and the boundary condition. Among the regularization models that have attracted a revived interest and considerable amount of attention in the tensor recovery literature are the low-rank prior, the sparsity regularization, and the nonlocal self similarity. Thus, incorporating these priors' knowledge in a unified regularizer has caught the attention of the imaging community. Therefore, in this

work, we consider a low-rank tensor learning with nonlocal weighted sparsity model for the denoising step. Moreover, we develop a joint deblurring and denoising method for tensor restoration problem.

3.1.1. ***Deblurring step: The computation of*** $\mathcal{P}_{\mathcal{K}}$ ***problem.*** We start with the deblurring step given by the minimization problem $\mathcal{P}_{\mathcal{K}}$

$$\hat{\mathcal{X}}^{(i)} = \arg\min_{\mathcal{X}} \|\mathcal{Y} - \mathcal{X} * \mathcal{K}\|_F^2 + \mu\|\mathcal{X} - \mathcal{X}^{(i-1)}\|_F^2 \tag{4}$$

This is a least square problem which leads to a close-form solution for $\hat{\mathcal{X}}^{(i)}$. The solution can be efficiently computed by the 3D fast Fourier transforms (3D FFT). Thus, in the Fourier domain, $\mathcal{P}_{\mathcal{K}}$ can be transformed into the following problem:

$$\mathcal{F}(\hat{\mathcal{X}}^{(i)}) = \arg\min_{\mathcal{F}(\mathcal{X})} \|\mathcal{F}(\mathcal{Y}) - \mathcal{F}(\mathcal{X}) \circ \mathcal{F}(\mathcal{K})\|_F^2 + \mu \left\| \mathcal{F}(\mathcal{X}) - \mathcal{F}(\mathcal{X}^{(i-1)}) \right\|_F^2. \tag{5}$$

$\mathcal{F}(.)$ denotes the 3D discrete Fourier transform and the operator $\circ$ is element-wise multiplication. The solution $\hat{\mathcal{X}}^{(i)}$ is given as follows:

$$\hat{\mathcal{X}}^{(i)} = \mathcal{F}^{-1}\left(\frac{\mathcal{F}^*(\mathcal{K}) \circ \mathcal{F}(\mathcal{Y}) + \mu\mathcal{F}(\mathcal{X}^{(i-1)})}{\mathcal{F}^*(\mathcal{K}) \circ \mathcal{F}(\mathcal{K}) + \mu\mathcal{I}}\right) \tag{6}$$

where $\mathcal{F}^*$ and $\mathcal{F}^{-1}$ are the conjugate of the FFT and its inverse respectively.

3.1.2. ***Denoising step: Low-rank tensor learning with nonlocal weighted sparsity model.*** Let us now return to the denoising step. As mentioned above, we consider a low-rank learning based nonlocal weighted sparsity denoising model. The approximation of the proposed regularization term consists of three steps namely, the patch grouping, low-rankness property, and the sparse constraint. Before providing the explicit form of the penalty term, we will present a brief overview of each of the three steps.

- **Patch extraction and grouping:** Given a third-order tensor $\mathcal{X} \in \mathbb{R}^{n_1,n_2,n_3}$, we denote by $\mathcal{G}_p$ the operator that extracts nonlocal similar overlapping 3-D patches from the tensor $\mathcal{X}$, where $\mathcal{G}_p\mathcal{X}$ is the constructed 3-order tensor for each exemplar cubic at location p. For each reference cubic patch with size $s \times s \times k$ in the whole 3-D images, we search for its similar cubic patches among adjacent cubic in a local window using block matching. After patch grouping, we unfold each 3-D patch into a 2-D matrix. Finally, these 2-D matrix is stacked into several clusters, which can be represented by a 3rd-order tensor. Let N be the number of the nonlocal similar patches, the obtained 3-order tensor is of the size $s^2 \times (N+1) \times k$ where $s^2 \times k$ is the size of the matricization cubic.
- **Low rank property:** In many applications, one wants to approximate a data matrix with a low-rank matrix. The SVD does this in the best way. The SVD is useful whenever we have a two-dimensional data set, which is naturally expressed in terms of a matrix. In the tensor view, the generalization of the SVD to higher order tensors has been developed in several ways. One main approach is the so-called high order singular value decomposition (HOSVD). Therefore, the constructed tensor is then characterized by a low-rank approximation via the HOSVD given as:

$$\mathcal{G}_p\mathcal{X} = \mathcal{D}_p \times_1 \boldsymbol{V}_{(1,p)} \times_2 \boldsymbol{V}_{(2,p)} \times_3 \boldsymbol{V}_{(3,p)} \tag{7}$$

Then, by summing over all clusters and averaging the results, the original $\mathcal{X}$ can be expressed as

$$\mathcal{X} = \left(\sum_p \mathcal{G}_p^T \mathcal{G}_p \right)^{-1} \sum_p \mathcal{G}_p^T \quad \mathcal{D}_p \times_1 \boldsymbol{V}_{(1,p)} \times_2 \boldsymbol{V}_{(2,p)} \times_3 \boldsymbol{V}_{(3,p)} \tag{8}$$

- **Sparsity constraint:** The estimation of the core tensor $\mathcal{D}_p$ is a severely ill-posed problem. To overcome this draw, the regularization method is considered. In this regard, sparse regularization, which refers to a process of introducing additional sparse constraint information in order to solve an ill-posed problem, has been efficiently exploited in several applications. Herein, the l_1-norm constraint is defined as the sum of absolute values of elements has been widely used. However, the l_1-norm regularization fairly penalizes all the components of the underlying data. Thus, replacing the l_1-norm with weighted l_1-norm has demonstrated to enhance the sparsity of the solution and improve the signal recovery performance [1]. Therefore, the proposed low-rank based sparsity regularization can be represented as:

$$\mathcal{J}(\mathcal{X}) = \sum_p \left\| \mathcal{G}_p \mathcal{X} - \mathcal{D}_p \times_1 \boldsymbol{V}_{(1,p)} \times_2 \boldsymbol{V}_{(2,p)} \times_3 \boldsymbol{V}_{(3,p)} \right\|_F^2 + \gamma \left\| \mathcal{D}_p \right\|_{\mathcal{W},1} \tag{9}$$

where $\|\mathcal{D}_p\|_{\mathcal{W},1} = \sum_{ijk} |w_{ijk} \mathcal{D}_p(i,j,k)|$, and w_{ijk} is positive weight. To promote the same sparsity structure in the solution that is present in the original tensor,w_{ijk} are selected such that they have small values on the nonzero locations and significantly larger values otherwise. Actually, information about the locations of the nonzero coefficients is not available, the critical task of selecting the weights is performed iteratively via iterative reweighting. The idea is to recompute weights at every iteration using the update of $\mathcal{D}_p$ at the previous iteration. Let t be the iteration reweighted counter, using an appropriate choice of positive values for parameters c and ε, we have

$$w_{i,j,k} = \frac{c}{|\mathcal{D}_p^t(i,j,k)| + \varepsilon} \tag{10}$$

Therefore, the denoising problem $\mathcal{P}_\mathcal{J}$ is given as follows:

$$\mathcal{P}_\mathcal{J} \; : \begin{cases} \left\{ \mathcal{D}_p, \boldsymbol{V}_{(j,p)} \right\} = \underset{\mathcal{D}_p, \boldsymbol{V}_{(j,p)}}{\arg\min} \sum_p \left\| \mathcal{G}_p \mathcal{X}^{(i-1)} - \mathcal{D}_p \times_1 \boldsymbol{V}_{(1,p)} \times_2 \boldsymbol{V}_{(2,p)} \times_3 \boldsymbol{V}_{(3,p)} \right\|_F^2 \\ \qquad\qquad + \gamma \left\| \mathcal{D}_p \right\|_{\mathcal{W},1} \\ \mathcal{X}^{(i)} = \underset{\mathcal{X}}{\arg\min} \| \mathcal{X} - \hat{\mathcal{X}}^{(i)} \|_F^2 + \lambda \sum_p \left\| \mathcal{G}_p \mathcal{X} - \mathcal{D}_p \times_1 \boldsymbol{V}_{(1,p)} \times_2 \boldsymbol{V}_{(2,p)} \times_3 \boldsymbol{V}_{(3,p)} \right\|_F^2 . \end{cases} \tag{11}$$

The computation of $\mathcal{P}_\mathcal{J}$ problem.

- **updating $(\mathcal{D}_p, \boldsymbol{V}_{(j,p)})$:** The usual strategy to solve the first equation in problem (11) is by using an alternating procedure which basically consists in alternatively learning the core tensor $\mathcal{D}_p$ approximation when the $\boldsymbol{V}_{(j,p)}$ is considered fixed and then in updating the $\boldsymbol{V}_{(j,p)}$ with the current $\mathcal{D}_p$. In doing so, updating the core tensor $\mathcal{D}_p$ can be given by:

$$\mathcal{D}_p = \underset{\mathcal{D}_p}{\arg\min} \left\| \mathcal{G}_p \mathcal{X} - \mathcal{D}_p \times_1 \boldsymbol{V}_{(1,p)} \times_2 \boldsymbol{V}_{(2,p)} \times_3 \boldsymbol{V}_{(3,p)} \right\|_F^2 + \gamma \left\| \mathcal{D}_p \right\|_{\mathcal{W},1} \tag{12}$$

it's closed solution can be directly given by the following equation:

$$\mathcal{D}_p = \text{shrink}_1\left(\mathcal{C}_p, \mathcal{W}_p \odot \gamma\right) \tag{13}$$

where

$$\mathcal{C}_p = \mathcal{G}_p\mathcal{X} \times_1 \boldsymbol{V}_{(1,p)}^T \times_2 \boldsymbol{V}_{(2,p)}^T \times_3 \boldsymbol{V}_{(3,p)}^T \tag{14}$$

and

$$[\text{shrink}_1(\mathcal{X}, \xi)]_{i,j,k} = \text{sign}\left(x_{i,j,k}\right) \max\left(|x_{i,j,k}| - \xi, 0\right) \tag{15}$$

Now, the sub-problem of updating the singular factors $\boldsymbol{V}_{(j,p)}$, $\{j = 1, 2, 3\}$ is given by:

$$\boldsymbol{V}_{(j,p)} = \underset{\boldsymbol{V}_{(j,p)}}{\arg\min} \sum_p \left\|\mathcal{G}_p\mathcal{X} - \mathcal{D}_p \times_1 \boldsymbol{V}_{(1,p)} \times_2 \boldsymbol{V}_{(2,p)} \times_3 \boldsymbol{V}_{(3,p)}\right\|_F^2 \tag{16}$$

Each $\boldsymbol{V}_{(j,p)}$, $\{j = 1, 2, 3\}$ can be solved independently. First, let $\mathcal{M} = \mathcal{G}_p\mathcal{X}$ and without loss of generality, we take $\boldsymbol{V}_{(1,p)}$ as an example, by unfolding the preceding problem according to the first direction, we have the equivalent minimization problem

$$\boldsymbol{V}_{(1,p)} = \underset{\boldsymbol{V}_{(1,p)}}{\arg\min} \left\|\mathcal{M}_{(1)} - \boldsymbol{V}_{(1,p)}\text{Unfold}_1\left(\mathcal{D}_p \times_2 \boldsymbol{V}_{(2,p)} \times_3 \boldsymbol{V}_{(3,p)}\right)\right\|_F^2 \tag{17}$$

by remark 2.1, the equation (17) is equivalent to

$$\max_{\boldsymbol{V}_{(1,p)}^T \boldsymbol{V}_{(1,p)} = \boldsymbol{I}} \left\langle \mathcal{L}_{(1)}, \boldsymbol{V}_{(1,p)} \right\rangle \tag{18}$$

where

$$\mathcal{L}_{(1)} = \left(\mathcal{M}_{(1)}\text{Unfold}_1\left(\mathcal{D}_p \times_2 \boldsymbol{V}_{(2,p)} \times_3 \boldsymbol{V}_{(3,p)}\right)\right). \tag{19}$$

In the same way we can see that the factors $\boldsymbol{V}_{(2,p)}$ and $\boldsymbol{V}_{(3,p)}$ can be updated by solving the following problem

$$\max_{\boldsymbol{V}_{(j,p)}^T \boldsymbol{V}_{(j,p)} = \boldsymbol{I}} \left\langle \mathcal{L}_{(j)}, \boldsymbol{V}_{(j,p)} \right\rangle \tag{20}$$

Finally, by using theorem 2.1 the solution of each $\boldsymbol{V}_{(j,p)}$, $\{j = 1, 2, 3\}$ can be given by the following matrix formula:

$$\boldsymbol{V}_{(j,p)}^+ = \boldsymbol{B}_j \boldsymbol{C}_j^T \tag{21}$$

where $\mathcal{L}_{(j)} = \boldsymbol{B}_j \boldsymbol{D} \boldsymbol{C}_j^T$ is the SVD decomposition of $\mathcal{L}_{(j)}$.

- **updating $\mathcal{X}^{(i)}$:** We turn now to compute the solution $\mathcal{X}^{(i)}$ which is obtained by solving the following quadratic optimization problem

$$\underset{\mathcal{X}}{\arg\min} \left\{ \|\mathcal{X} - \hat{\mathcal{X}}^{(i)}\|_F^2 + \lambda \sum_p \left\|\mathcal{G}_p\mathcal{X} - \mathcal{D}_p \times_1 \boldsymbol{V}_{(1,p)} \times_2 \boldsymbol{V}_{(2,p)} \times_3 \boldsymbol{V}_{(3,p)}\right\|_F^2 \right\} \tag{22}$$

Setting the derivative of the above problem to zero with respect to $\mathcal{X}$, we obtain the following closed solution

$$\mathcal{X}^{(i)} = \left(\mathcal{I} + \lambda \sum_p \mathcal{G}_p^T \mathcal{G}_p\right)^{-1} \left(\hat{\mathcal{X}}^{(i)} + \lambda \sum_p \mathcal{G}_p^T \quad \mathcal{D}_p \times_1 \boldsymbol{V}_{(1,p)} \times_2 \boldsymbol{V}_{(2,p)} \times_3 \boldsymbol{V}_{(3,p)}\right) \tag{23}$$

4. Results and discussion

This section is devoted to numerically evaluating the effectiveness of the proposed method on deblurring three-way tensors. We compare the proposed method with three current state-of-the-art HSI deblurring methods including FPD [16], SSTV [12], and DB-WLRTR [4]. In fast positive deconvolution (FPD) method, an efficient approach performing deconvolution of large hyperspectral images under a positivity constraint is presented. In the SSTV approach, an hyperspectral image deconvolution method based on spectral-spatial total variation prior and nonnegative constraint is exploited to obtain the restored images. In [4], the nonlocal similarity within spectral-spatial cubic and spectral correlation are both represented simultaneously. For this work, we are interested only to the deblurring section, since the manuscript describes several restoration tasks.

In the experiments, we consider a set of test problems, where the data are obtained by convoling the image with a point spread function (PSF) with a boundary condition. To demonstrate the efficiency of our strategy against various types of degradation, we test the proposed algorithm and compare it with other restoration methods using two blurring kernels, Gaussian blur kernel of size 8×8 with standard deviation 3 and averaging blur of size 12. The two kernels are generated using the Matlab functions *fspecial('gaussian',8*8,3)* and *fspecial('average',12)*, respectively. Moreover, the peak signal-to-noise rate (PSNR) and the structural similarity index (SSIM) [25] are used as a criterion for evaluating the quality of the reconstructed results.

In this section, we test seven data sets, including egyptian statue [1], cloth [1], chart and stuffed toys[1], stuffed toys[1], origami[2], spray[2], and butterfly2[2] data set. In our tests, we select a part of them (of size $256 \times 256 \times 31$) for the four first images, and a portion of size $256 \times 256 \times 30$ of last tree images.

Table 1 summarizes the PSNR and SSIM values achieved by the reconstructed results of the four deblurring methods for the Gaussian kernel. In terms of both PSNR and SSIM values, results demonstrate that the proposed method consistently outperforms the comparative methods. Similarly, under the averaging blur, from the PSNR and SSIM values presented in Table 2, we can see that the proposed method achieves higher values comparing to the other deblurring methods.

For comprehensive comparisons of the performance of the four utilized deblurring methods for Gaussian and averaging kernels, we consider four reconstructed images egyptian statue, cloth, origami, spray as representations. We have displayed one frame of all reconstructed images. To further compare the visual results, in Figure 1 to Figure 8, we have zoomed different regions in images to compare the significance of the four methods in recovering local details. In Figures 1,3,5,7, we illustrate the original, degraded image by gaussian kernel, resulted image using FPD, SSTV, DB-WLRTR methods, and the reconstructed image using our method. Similarly, in Figures 2,4,6,8, we display the original, the degraded image by averaging kernel, the resulted image using FPD, SSTV, DB-WLRTR approaches, and the reconstructed image using our method.

[1] https://www.cs.columbia.edu/CAVE/databases/multispectral/
[2] http://www.ok.sc.e.titech.ac.jp/res/MSI/MSIdata59.html

TABLE 1. The PSNR/SSIM obtained by the reconstruction of different images degraded by gaussian kernel. For each test, four results are provided FPD, SSTV, DB-WLRTR, and our proposed method.

Images	Measures	Methods			
		FPD	SSTV	DB-WLRTR	Our method
egyptian statue	PSNR	29.525	36.498	55.205	**59.043**
	SSIM	0.9438	0.9669	0.9989	**0.9996**
cloth	PSNR	30.024	31.263	46.116	**50.289**
	SSIM	0.8950	0.8226	0.9918	**0.9966**
chart and stuffed toy	PSNR	23.015	28.237	48.855	**52.776**
	SSIM	0.8942	0.8517	0.9972	**0.9988**
stuffed toys	PSNR	26.036	41.496	55.585	**57.546**
	SSIM	0.9682	0.9780	0.9986	**0.9992**
Origami	PSNR	24.835	30.999	51.187	**56.191**
	SSIM	0.9230	0.9017	0.9979	**0.9992**
Spray	PSNR	22.601	26.359	43.696	**50.403**
	SSIM	0.8985	0.8133	0.9953	**0.9986**
Butterfly2	PSNR	16.880	32.967	51.318	**55.410**
	SSIM	0.8247	0.9411	0.9981	**0.9990**

TABLE 2. The PSNR/SSIM obtained by the reconstruction of different images degraded by averaging kernel. For each test, four results are provided FPD, SSTV, DB-WLRTR, and our proposed method.

Images	Measures	Methods			
		FPD	SSTV	DB-WLRTR	Our method
egyptian statue	PSNR	26.811	34.992	54.494	**57.550**
	SSIM	0.8429	0.9388	0.9984	**0.9994**
cloth	PSNR	25.332	29.902	43.250	**43.259**
	SSIM	0.5887	0.7606	0.9808	**0.9814**
chart and stuffed toy	PSNR	18.485	26.819	48.340	**51.038**
	SSIM	0.5791	0.7991	0.9969	**0.9980**
stuffed toys	PSNR	22.398	37.743	55.059	**56.956**
	SSIM	0.8558	0.9481	0.9984	**0.9990**
Origami	PSNR	19.653	28.376	49.297	**54.317**
	SSIM	0.6308	0.7982	0.9973	**0.9984**
Spray	PSNR	18.557	25.609	41.660	**44.859**
	SSIM	0.4839	0.7815	0.9910	**0.9943**
Butterfly2	PSNR	14.817	29.683	50.525	**54.304**
	SSIM	0.7271	0.8702	0.9977	**0.9986**

We observe that the visual effect of the reconstructed image by the proposed method is quite good and is comparable to the other tree restoration methods especially comparing to FPD and SSTV results. The proposed approach is capable to efficiently generating the image edges and textures. Clearly, our method is able to recover the losing details in the degraded images.In contrast, the results obtained

by FPD and SSTV contain evident blurry area, leading to losing some details. On the other hand, DB-WLRTR can perform comparatively better in deblurring image with respect to FPD and SSTV. However, comparing with our algorithm, we can see from the enlarged parts that our approach restore more details, whilst visually the results may look similar. In several tests, we can remark that the zoomed regions in the DB-WLRTR results present some imperfections. For example, in Figure 1. if we observe deeply, we can easily notice that fine details are distorted and there has some considerable artifacts. Besides, in Figures 3 and 4, it is seen that the symbol illustrated the zoomed part of the results of DB-WLRTR is not clear as for our results whether under the gaussian or averaging kernels. Moreover, It is well-known that, higher PSNR and SSIM indicates higher reconstruction quality. In this context, PSNR and SSIM values of our algorithm are larger in overall test.

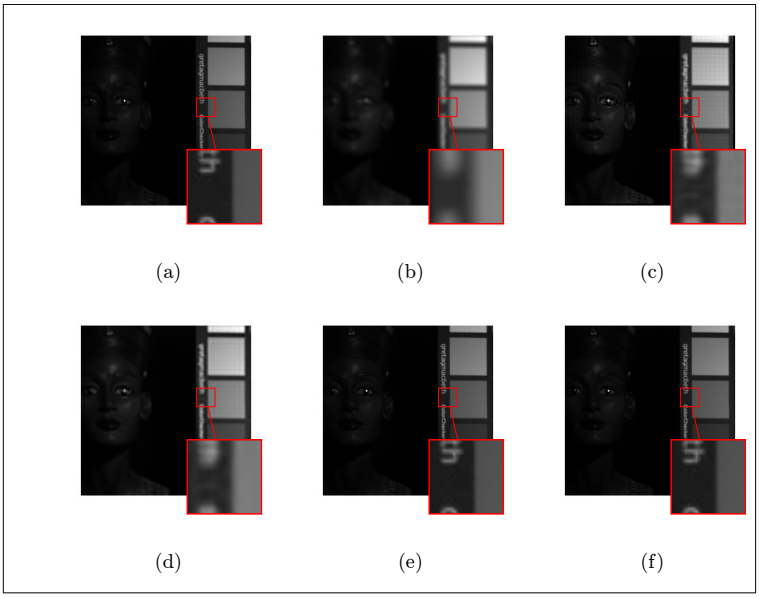

FIGURE 1. The visual comparison results of the recovered *egyptian* image. (a) The original image at band 6, (b) The degraded image by kernel 1, The recovered results by (c) FPD, (d) SSTV, (e) DB-WLRTR, and (f) the proposed method, respectively.

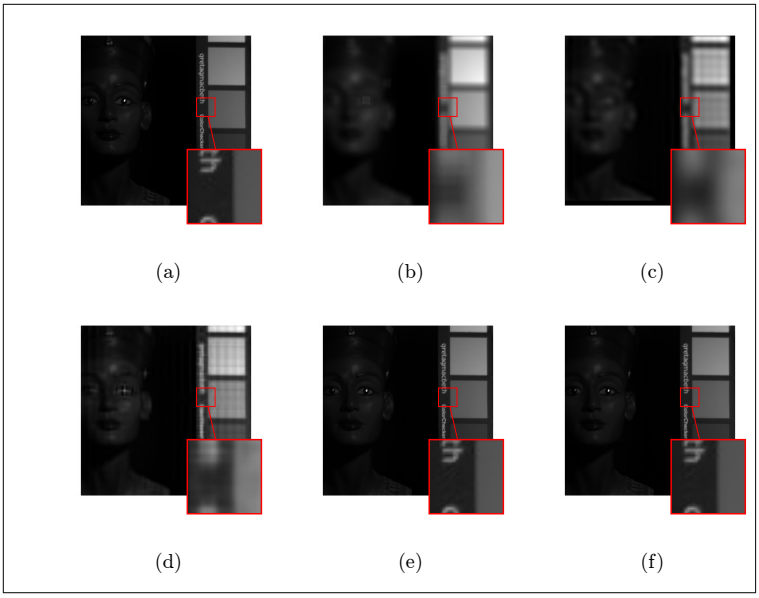

FIGURE 2. The visual comparison results of the recovered *egyptian* image. (a) The original image at band 3, (b) The degraded image by kernel 2, The recovered results by (c) FPD, (d) SSTV, (e) DB-WLRTR, and (f) the proposed method, respectively.

5. Conclusion

In this paper, we have proposed an effective iterative algorithm based on a decoupled method for multidimensional image deblurring problem. The idea is to split the objective function into two iterative minimization problems. Thus, we obtain a simple deblurring problem based on a model denoiser. The nonlocal low rank and weighted sparsity regularization is employed, is the core of the deblurring process. The suggested approach outperforms the other classical methods in literature via extensive numerical experiments. Our method can be extended to consider other denoising model in the aim to enhance the deblurring step.

References

[1] M.S. Asif, J. Romberg, Fast and accurate algorithms for re-weighted l1-norm minimization, *IEEE Transactions on Signal Processing* **61** (2013), no. 23, 5905-5916.

[2] O. Banouar, S. Mohaoui, S. Raghay, Collaborating filtering using unsupervised learning for image reconstruction from missing data, *EURASIP Journal on Advances in Signal Processing* **2018** (2018), no. 1, 1-12.

[3] A. Beck, M. Teboulle, Fast gradient-based algorithms for constrained total variation image denoising and deblurring problems, *IEEE transactions on image processing* **18** (2009), no. 11, 2419-2434.

[4] Y. Chang, L. Yan, X.-L. Zhao, H. Fang, Z. Zhang, S. Zhong, Weighted low-rank tensor recovery for hyperspectral image restoration, *IEEE transactions on cybernetics* **50** (2020), no. 11, 4558-4572.

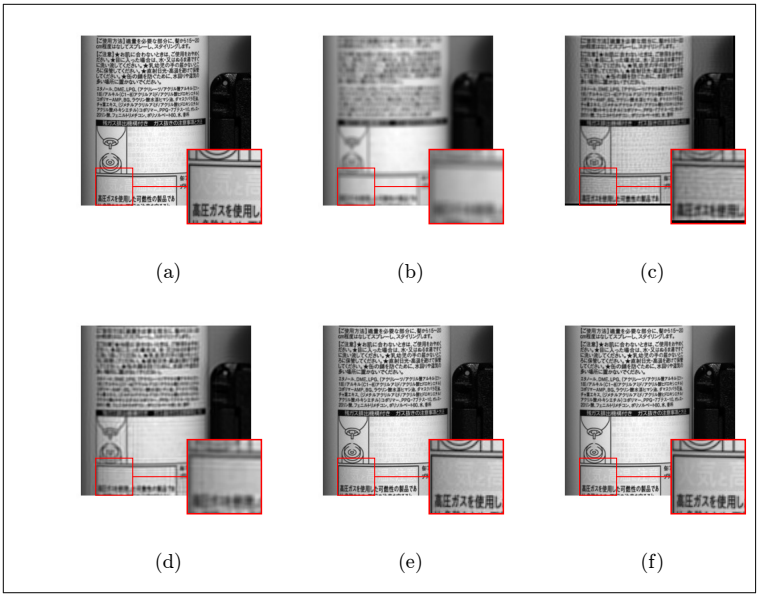

FIGURE 3. The visual comparison results of the recovered *Spray* image. (a) The original image at band 24, (b) The degraded image by kernel 1, The recovered results by (c) FPD, (d) SSTV, (e) DB-WLRTR, and (f) the proposed method, respectively.

[5] Y. Chen, W. He, N. Yokoya, T.-Z. Huang, X.-L. Zhao, Nonlocal tensor-ring decomposition for hyperspectral image denoising, *IEEE Transactions on Geoscience and Remote Sensing* **58** (2019), no. 2, 1348-1362.

[6] A. Cichocki, R. Zdunek, A. H. Phan, S.-I. Amari, *Nonnegative matrix and tensor factorizations: applications to exploratory multi-way data analysis and blind source separation*, John Wiley & Sons, 2009.

[7] W. Dong, G. Shi, X. Li, Image deblurring with low-rank approximation structured sparse representation, In: *Proceedings of the 2012 Asia Pacific Signal and Information Processing Association Annual Summit and Conference* (2012), IEEE, 1-5.

[8] E.M. Eksioglu, Decoupled algorithm for MRI reconstruction using nonlocal block matching model: BM3D-MRI, *Journal of Mathematical Imaging and Vision* **56** (2016), no. 3, 430-440.

[9] K. El Qate, M. El Rhabi, A. Hakim, E. Moreau, N. Thirion-Moreau, Hyperspectral image completion via tensor factorization with a bi-regularization term, *Journal of Signal Processing Systems* **2022** (2022), 1-11.

[10] K. El Qate, M. El Rhabi, A. Hakim, E. Moreau, N. Thirion-Moreau, A primal-dual algorithm for nonnegative N-th order CP tensor decomposition: application to fluorescence spectroscopy data analysis, *Multidimensional Systems and Signal Processing* **33** (2022), no. 2, 665-682.

[11] K. EL Qate, S. Mohaoui, A. Hakim, S. Raghay, Color image completion using tensor truncated nuclear norm with l0 total variation, *Annals of the University of Craiova-Mathematics and Computer Science Series* **49** (2022), no. 2, 250-259.

[12] H. Fang, C. Luo, G. Zhou, X. Wang, Hyperspectral image deconvolution with a spectral-spatial total variation regularization, *Canadian Journal of Remote Sensing* **43** (2017), no. 4, 384-395.

[13] S. Gu, L. Zhang, W. Zuo, X. Feng, Weighted nuclear norm minimization with application to image denoising, In: *Proceedings of the IEEE conference on computer vision and pattern recognition* (2014), 2862-2869.

[14] R. Hao, Z. Su, A patch-based low-rank tensor approximation model for multiframe image denoising, *Journal of Computational and Applied Mathematics* **329** (2018), 125-133.

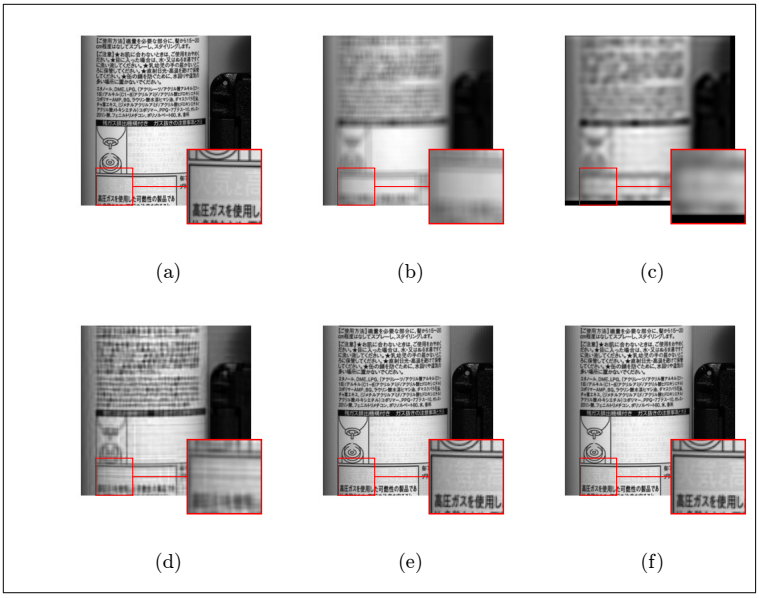

FIGURE 4. The visual comparison results of the recovered *Spray* image. (a) The original image at band 24, (b) The degraded image by kernel 2, The recovered results by (c) FPD, (d) SSTV, (e) DB-WLRTR, and (f) the proposed method, respectively.

[15] W. He, H. Zhang, L. Zhang, H. Shen, Hyperspectral image denoising via noise-adjusted iterative low-rank matrix approximation, *IEEE Journal of Selected Topics in Applied Earth Observations and Remote Sensing* **8** (2015), no. 6, 3050-3061.

[16] S. Henrot, C. Soussen, D. Brie, Fast positive deconvolution of hyperspectral images, *IEEE Transactions on Image Processing* **22** (2012), no. 2, 828-833.

[17] T. Korah, C. Rasmussen, Spatiotemporal inpainting for recovering texture maps of occluded building facades, *IEEE Transactions on Image Processing* **16** (2007), no. 9, 2262-2271.

[18] N. Kreimer, M.D. Sacchi, A tensor higher-order singular value decomposition for prestack seismic data noise reduction and interpolation, *Geophysics* **77** (2012), no. 3, V113-V122.

[19] N. Li, B. Li, Tensor completion for on-board compression of hyperspectral images, In: *2010 IEEE International Conference on Image Processing* (2010), IEEE, 517-520.

[20] S. Mohaoui, A. Hakim, S. Raghay, Tensor completion via bilevel minimization with fixed-point constraint to estimate missing elements in noisy data, *Advances in Computational Mathematics* **47** (2021), no. 1, 1-27.

[21] T. Poggio, V. Torre, Ill-posed problems and regularization analysis in early vision, Technical report, MASSACHUSETTS INST OF TECH CAMBRIDGE ARTIFICIAL INTELLIGENCE LAB, 1984.

[22] W. Ren, X. Cao, J. Pan, X. Guo, W. Zuo, M.-H. Yang, Image deblurring via enhanced low-rank prior, *IEEE Transactions on Image Processing* **25** (2016), no. 7, 3426-3437.

[23] Y. Tang, Y. Xue, Y. Chen, L. Zhou, Blind deblurring with sparse representation via external patch priors, *Digital Signal Processing* **78** (2018), 322-331.

[24] X. Tao, H. Gao, X. Shen, J. Wang, J. Jia, Scale-recurrent network for deep image deblurring, In: *Proceedings of the IEEE Conference on Computer Vision and Pattern Recognition* (2018), 8174-8182.

[25] Z. Wang, A.C. Bovik, H.R. Sheikh, E.P. Simoncelli, Image quality assessment: from error visibility to structural similarity, *IEEE transactions on image processing* **13** (2004), no. 4, 600-612.

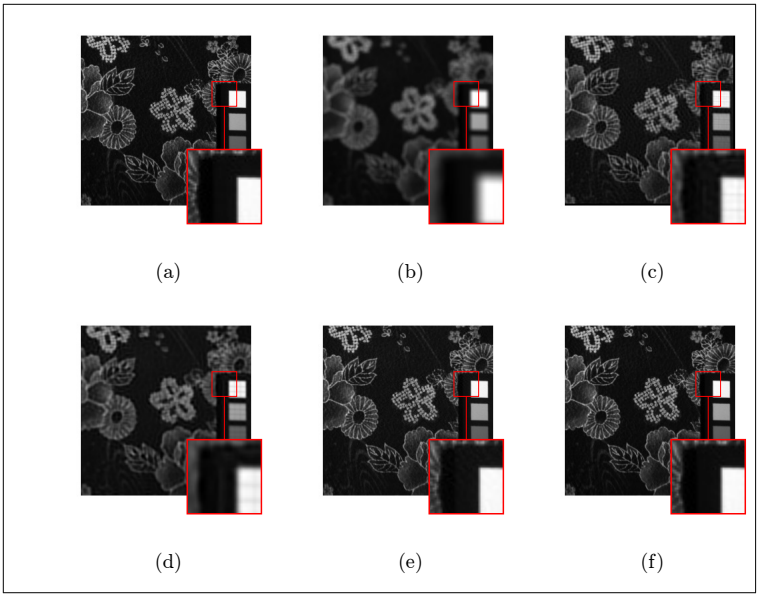

FIGURE 5. The visual comparison results of the recovered *Cloth* image. (a) The original image at band 5, (b) The degraded image by kernel 1, The recovered results by (c) FPD, (d) SSTV, (e) DB-WLRTR, and (f) the proposed method, respectively.

[26] Y.-W. Wen, M.K. Ng, W.-K. Ching, Iterative algorithms based on decoupling of deblurring and denoising for image restoration, *SIAM Journal on Scientific Computing* **30** (2008), no. 5, 2655-2674.

[27] Q. Xie, Q. Zhao, D. Meng, Z. Xu, S. Gu, W. Zuo, L. Zhang, Multispectral images denoising by intrinsic tensor sparsity regularization, In: *Proceedings of the IEEE conference on computer vision and pattern recognition* (2016), 1692-1700.

[28] Y. Xie, Y. Qu, D. Tao, W. Wu, Q. Yuan, W. Zhang, Hyperspectral image restoration via iteratively regularized weighted schatten p-norm minimization, *IEEE Transactions on Geoscience and Remote Sensing* **54** (2016), no. 8, 4642-4659.

[29] J. Xu, L. Zhang, W. Zuo, D. Zhang, X. Feng, Patch group based nonlocal self-similarity prior learning for image denoising, In: *Proceedings of the IEEE international conference on computer vision* (2015), 244-252.

[30] H. Zhang, Y. Dai, H. Li, P. Koniusz, Deep stacked hierarchical multi-patch network for image deblurring, In: *Proceedings of the IEEE/CVF Conference on Computer Vision and Pattern Recognition* (2019), 5978-5986.

[31] H. Zhou, Y. Su, Z. Li, Hyperspectral mixed noise removal via subspace representation and weighted low-rank tensor regularization, arXiv preprint arXiv:2111.07044 (2021).

(Karima El Qate, Souad Mohaoui) CADI AYYAD UNIVERSITY FACULTY OF SCIENCE AND TECHNICS GUILIZ, MARRAKESH
E-mail address: karima.elqate@gmail.com, souad.mohaoui@gmail.com

(Abdelilah Hakim, Said Raghay) CADI AYYAD UNIVERSITY FACULTY OF SCIENCE AND TECHNICS GUILIZ, MARRAKESH
E-mail address: abdelilah.hakim@gmail.com, s.raghay@uca.ma

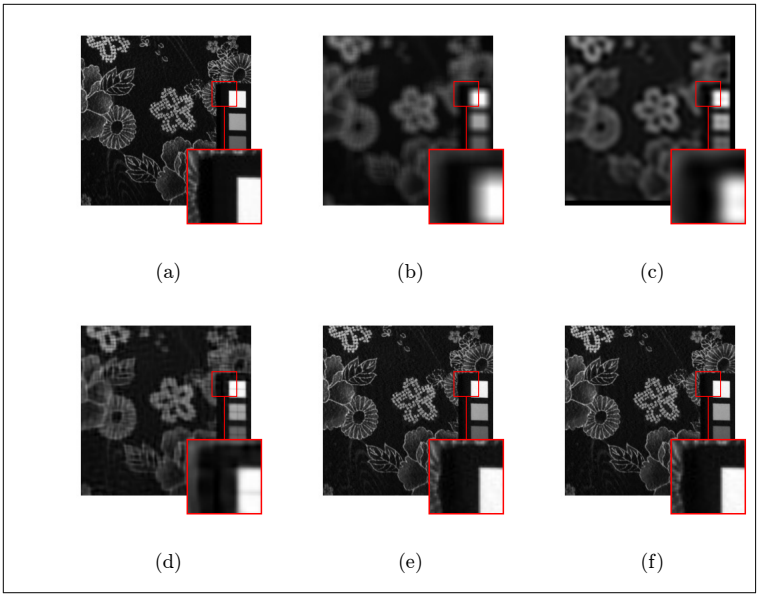

FIGURE 6. The visual comparison results of the recovered *Cloth* image. (a) The original image at band 5, (b) The degraded image by kernel 2, The recovered results by (c) FPD, (d) SSTV, (e) DB-WLRTR, and (f) the proposed method, respectively.

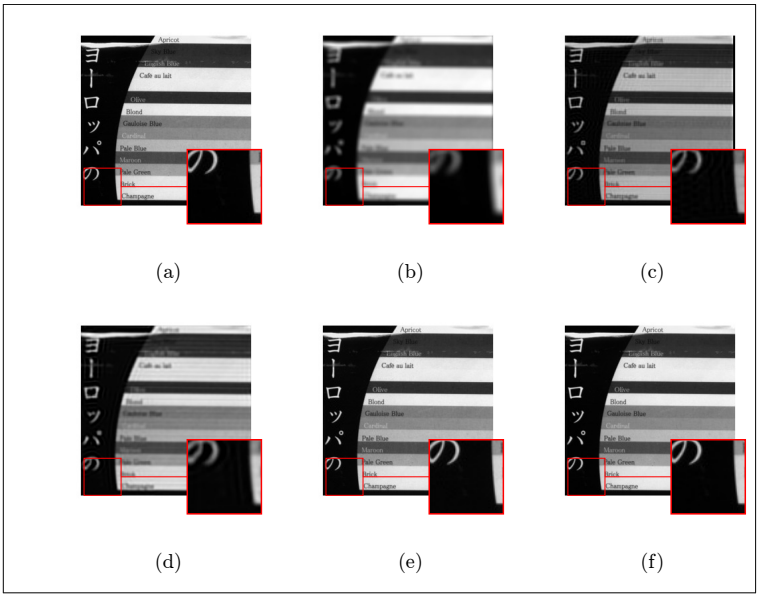

FIGURE 7. The visual comparison results of the recovered *Origami* image. (a) The original image at band 24, (b) The degraded image by kernel 1, The recovered results by (c) FPD, (d) SSTV, (e) DB-WLRTR, and (f) the proposed method, respectively.

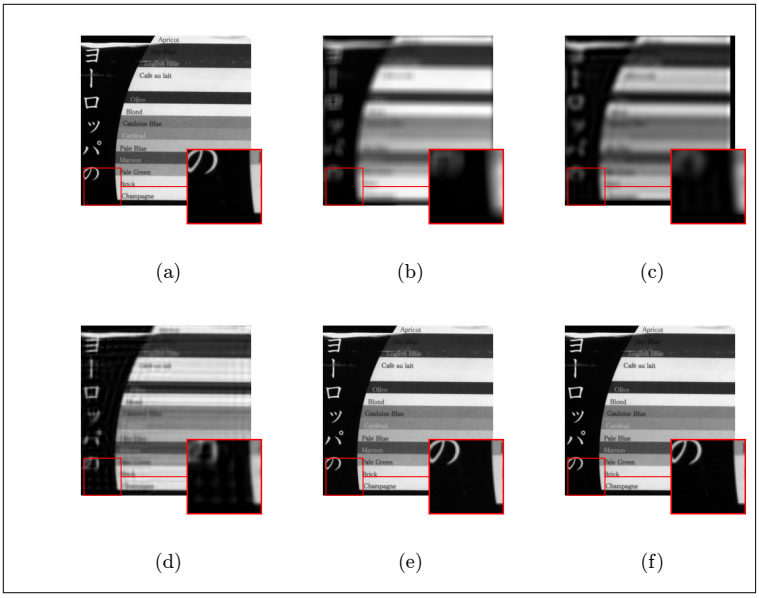

FIGURE 8. The visual comparison results of the recovered *Origami* image. (a) The original image at band 24, (b) The degraded image by kernel 2, The recovered results by (c) FPD, (d) SSTV, (e) DB-WLRTR, and (f) the proposed method, respectively.